

Modified black phosphorus quantum dots promotes spinal cord injury repair by targeting the AKT signaling pathway

Dong-Mei Xie³ , Chuanwei Sun¹,
Qingqiang Tu⁴, Suyi Li^{1,2}, Yu Zhang^{1,2}, Xifan Mei⁵
and Yuanlong Li^{1,2} 

Abstract

Spinal cord injury (SCI) is a serious refractory disease of the central nervous system (CNS), which mostly caused by high-energy trauma. Existing interventions such as hormone shock and surgery are insufficient options, which relate to the secondary inflammation and neuronal dysfunction. Hydrogel with neuron-protective behaviors attracts tremendous attention, and black phosphorus quantum dots (BPQDs) encapsulating with Epigallocatechin-3-gallate (EGCG) hydrogels (E@BP) is designed for inflammatory modulation and SCI treatment in this study. E@BP displays good stability, biocompatibility and safety profiles. E@BP incubation alleviates lipopolysaccharide (LPS)-induced inflammation of primary neurons and enhances neuronal regeneration in vitro. Furthermore, E@BP reconstructs structural versus functional integrity of spinal cord tracts, which promotes recovery of motor neuron function in SCI rats after transplantation. Importantly, E@BP restarts the cell cycle and induces nerve regeneration. Moreover, E@BP diminishes local inflammation of SCI tissues, characterized by reducing accumulation of astrocyte, microglia, macrophages, and oligodendrocytes. Indeed, a common underlying mechanism of E@BP regulating neural regenerative and inflammatory responses is to promote the phosphorylation of key proteins related to AKT signaling pathway. Together, E@BP probably repairs SCI by reducing inflammation and promoting neuronal regeneration via the AKT signaling pathway.

Keywords

Spinal cord injury, black phosphorus quantum dots, anti-inflammation, neuro-regeneration, AKT signaling pathway

Date received: 6 February 2023; accepted: 19 May 2023

¹Guangdong Cardiovascular Institute, Guangdong Provincial People's Hospital, Guangdong Academy of Medical Sciences, Southern Medical University, Guangzhou, China

²Department of Orthopedics, Guangdong Provincial People's Hospital, Guangdong Academy of Medical Sciences, Guangzhou, China

³Department of Cardiology, The Third Affiliated Hospital of Sun Yat-sen University, Guangzhou, China

⁴Zhongshan Medical College, Sun Yat-sen University, Guangzhou, China

⁵Department of Orthopedics, The Third Affiliated Hospital of Jinzhou Medical University, Jinzhou Medical University, Jinzhou, China

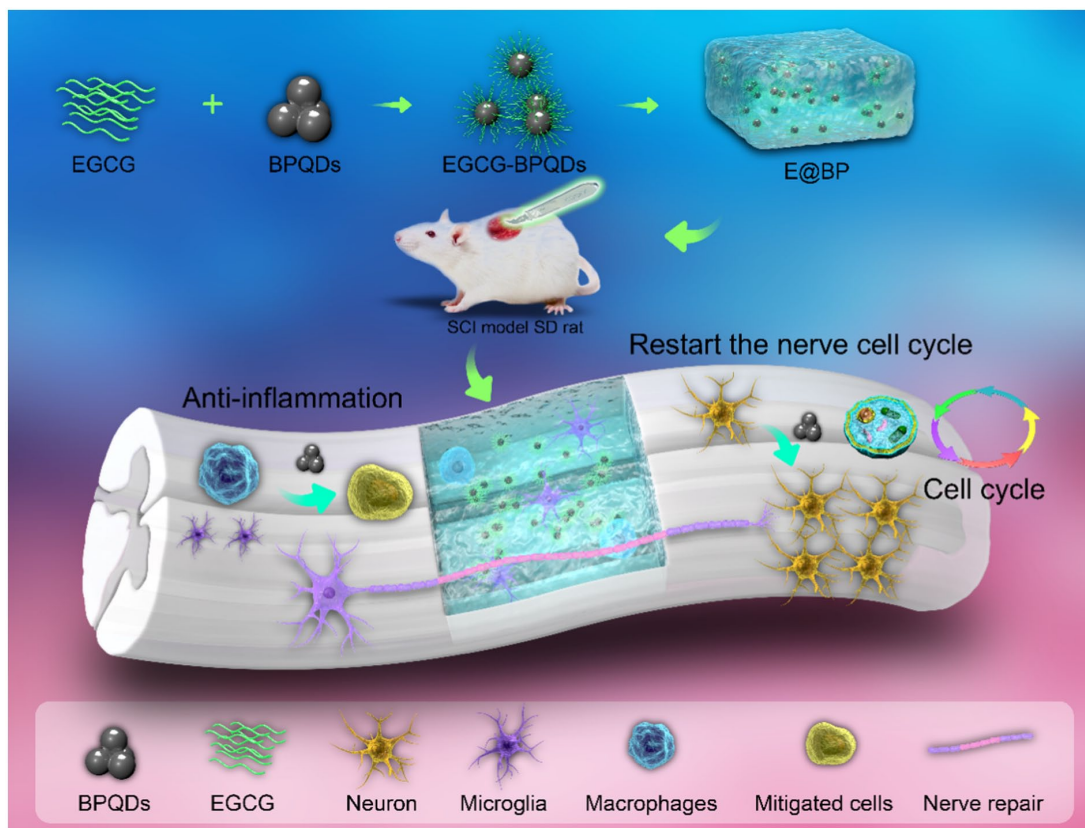
Corresponding authors:

Yuanlong Li, Department of Orthopedics, Guangdong Provincial People's Hospital, Guangdong Academy of Medical Sciences, Zhongshan Road 2, Guangzhou 510080, China.
Email: liyuanlong2015@foxmail.com

Xifan Mei, Department of Orthopedics, The Third Affiliated Hospital of Jinzhou Medical University, Jinzhou Medical University, Jinzhou 121001, China.
Email: meixifan1971@163.com

Yu Zhang, Department of Orthopedics, Guangdong Provincial People's Hospital, Guangdong Academy of Medical Sciences, Guangzhou 510080, China.
Email: luck_2001@126.com





TOC Text:

Black phosphorus quantum dots (BPQDs) encapsulating with EGCG hydrogels (E@BP) regulates neural regeneration and inflammatory by phosphorylating key proteins related to AKT signaling pathway in spinal cord injury rats.

Introduction

Spinal cord injury (SCI) is a variety of severe damages to the central nervous system (CNS), which impair the limbs below the damaged innervated nerve.¹ In China, the SCI incidence is 23.7–60.6 per million individuals.^{2,3} Accidental falls (31.8%) and road accidents (39.3%) are the two main causes of SCI. SCI drastically decreases patients' quality of life and is responsible for tremendous social versus economic burdens.⁴ Presently, clinical treatment for SCI involves surgical fenestration decompression and methylprednisolone (MP) shock therapy, whereas both treatments demonstrate limited therapeutic efficacy.^{5–7} Our previous research shown that the neuronal apoptosis and demyelination caused by inflammation in the SCI tissues disrupt fast SCI healing.^{8–10} The poor proliferation capacity of mature neurons also remains a great challenge to repair SCI.^{11,12} Thus, reducing local inflammatory responses and inducing neural proliferation have great potential to promote SCI healing. Myeloid mononuclear macrophages (especially microglia, a CNS resident macrophage) were activated post SCI, which trigger inflammatory reaction and aggravated the injury of the spinal cord tissue.^{13–15} Therefore, reducing the activity of macrophages and microglia in the injured area is supposed to promote SCI repair. MP therapy reduces

secondary injury to spinal cord caused by macrophages and microglia.¹⁶ However, MP arrested the cell cycle and reduced cell regeneration ability, these side effects limit its usage in clinic.^{17–20}

Black phosphorus (BP), a black crystal with a metallic luster, is formed by converting white phosphorus under high pressure and temperature.²¹ Interestingly, black phosphorus quantum dots (BPQDs) are one of new biodegradable nanomaterials and have many advantages, such as strong phosphorylation ability, tissue repair capacity, anti-inflammatory efficiency and low cytotoxicity properties.^{22,23} Critically, BPQDs can effectively induce neurogenesis and stimulate axon growth under mild oxidative stress, but the underlying molecular mechanism is unclear.²⁴ Studies indicated that neurons have effective self-repair mechanisms by re-entering the cell cycle.²⁵ However, it is believed that adult mature neuron is post-mitotic cell with extremely limited regenerative ability.^{25,26} Fortunately, the restart of the cell cycle in mature cells is mediated by specific regulatory proteins in the nucleus,^{27,28} and most of them are phosphorylated.^{29,30} Therefore, promoting the phosphorylation of the cell cycle-related proteins would effectively induce neural regeneration in the SCI site.

Interestingly, BPQDs have strong phosphorylation activity and alleviate SCI by promoting protein phosphorylation.^{23,24,31} It remains unclear whether BPQDs could effectively reduce inflammation, and whether BPQDs would promote neuronal regeneration after SCI. From the application perspective, the instability of BPQDs in the body is one of the difficulties, and processing BPQDs to spinal cord via advanced technology is also a key point. Previous studies have shown that hydrogels, carriers for nanomaterials, are widely used to construct stable drug dispersion system in medicine and tissue engineering.^{21,22} Here, we hypothesize that E@BP (EGCG hydrogel encapsulated BPQDs) could solve these two problems of BPQDs listed above.

In this study, black phosphorus quantum dots (BPQDs) encapsulating with Epigallocatechin-3-gallate (EGCG) hydrogels (E@BP) is designed for inflammatory modulation and SCI treatment. The effect of E@BP on the recovery of motor function in SCI rats was performed by the behavioral score. Regeneration and apoptosis of primary spinal cord neurons and glial were detected by immunofluorescence or flow cytometry. EDU and cell cycle-related proteins are regeneration related arrays. The inflammation-related protein chip was used to confirm the anti-inflammatory ability of E@BP on the SCI sites. Phosphorylated proteomics is applied to examine the molecular mechanism.

Materials and methods

Animals and experimental protocols

Male Sprague–Dawley rats (12 weeks old, 320–350 g) were purchased from the Guangdong Medical Laboratory Animal Center (SCHK [YUE] 2022-0002). The rats were housed in cages under specific pathogen-free (SPF) conditions. Animal maintenance and experimental protocols followed the NIH guidelines for the Care and Use of Laboratory Animals. The rats were randomly divided into four groups ($n=30$ per group), including sham group, SCI group, hydrogel group and E@BP group. In the sham group, the back tissue was blunt-dissected to destroy the lamina at the T9–10 segment without injuring the spinal cord. SCI (completely transection) model was induced in the SCI group, a laminectomy was performed to expose spinal cord segment T10 and inflict injury on T10 using ophthalmic scissors and.³² In the hydrogels group, the SCI model was induced as described, then hydrogel was evenly spread on the injured area. In the E@BP group, E@BP was evenly spread at the SCI area after SCI.

Preparation of black phosphorus quantum dots (BPQDs)

BPQDs (Xianfeng Nanomaterial Technology, Jiangsu, China) were synthesized using a liquid stripping method

that combines probe and water bath ultrasound. Briefly, 500 mg of powdered black phosphorus crystal was dispersed in 50 mL 1-Methyl-2-pyrrolidone (NMP) (Aladdin reagent, Shanghai, China) at 4°C. The solution was subjected to a 19–25 kHz probe-type ultrasonic device (19–25 kHz, 1200 W) for 4 h. The solution was centrifuged, and the upper solution was collected and sonicated overnight in an ice bath using a power of 300 W. The sample was centrifuged at 10,000 rpm for 20 min, and the supernatant containing BPQDs was decanted gently. The hydrogels were prepared through the following steps. Initially, 10 mL of 8% (w/v) polyvinyl alcohol solution was added to a beaker containing deionized water (10 mL). Next, 0.1 g sodium alginate powder was added to the beaker containing the polyvinyl alcohol solution. After mixing, the solution was incubated in a water bath at 50°C and stirred with a magnetic stirrer at 350 rpm for 1 h. The 10 mL suspension was dispersed in NMP at 13,000 rpm for 20 min, and the precipitates were again dispersed in a homogeneous hydrogel solution. After 25 min of ultrasonic treatment, the probe was aged for 6 h to obtain E@BP.

Characterization of the BPQDs

The morphology of BPQDs was observed by a transmission electron microscope (JEM-1200 EX, Tokyo, Japan). The particle size was characterized by dynamic laser scattering (DLS) (Malvern, Nano Z90, Worcestershire, UK). The composition of E@BP was assessed by Fourier transform infrared spectroscopy (FTIR) (Shimadzu, Kyoto, Japan). The fluorescence data (488 nm) were obtained by a fluorometer (F97PRO, Shanghai, China). The same PBS and water were kept throughout the experiment when assess the release profile of BPQDs. Finally, E@BP were characterized by differential scanning calorimetry (DSC) (DSC PT1600, LINSEIS, Germany).

Primary neuron treatment

Primary neurons isolated from the spinal cord of rat embryos (E16.5 day) were cultured in Dulbecco's Modified Eagle Medium (DMEM) (Gibco, MA, USA) without fetal bovine serum (FBS) (Gibco, MA, USA) for 6 h. Then, the cells were cultivated in Neurobasal media (Gibco, MA, USA) supplemented with 2% B27 (Gibco, MA, USA), and replaced with fresh medium every day. After 5-day culture, primary neurons were used for experiments. The primary neurons were randomly divided into three groups, the sham group: primary neurons without any treatment; Lipopolysaccharide (LPS) group: primary neurons treated with 100 ng/mL LPS (Sigma-Aldrich, MO, USA) for 24 h at 37°C; BPQDs group comprised primary neurons treated with BPQDs (24 h, 100 $\mu\text{g}\cdot\text{mL}^{-1}$) following LPS (24 h, 100 ng $\cdot\text{mL}^{-1}$) at 37°C.

BBB scores and angle of incline analysis

The motor function at 1, 2, 3, 4, 5, 6, 7, and 8 weeks after SCI was continuously evaluated via the Basso, Beattie, and Bresnahan scores (BBB scores). The BBB scores ranged from 0 (complete paralysis) to 21 (without injury), which based on the movement and coordination of ankles, hips, knees, and trunk.³³ In addition, the inclined plane test was used to evaluate the limb balance by placing the rats on a testing apparatus (a board covered with a rubber mat). The angle of the inclined plate could estimate the repair of hind limbs in rats.³⁴ BBB scoring and angle of incline were independently performed by three experienced researchers in a double-blind process.

Small animal imaging

The rats were sacrificed on 24, 36, 72h, and 96 h after SCI following intraperitoneal anesthetization with sodium pentobarbital, and the spinal cord was harvested. The spinal cord tissues were placed in an *IVIS Spectrum* imaging system (IVIS Spectrum, PerkinElmer, MA, USA), and the 488-channel laser was used to detect E@BP fluorescence intensity.

Immunofluorescence and immunohistochemical arrays

The primary neurons were washed twice with PBS and fixed with 4% PFA at 4°C overnight, and incubated with 10% goat serum containing 3% Triton 100 (T9284, Sigma-Aldrich, MO, USA) at room temperature for 3 h. After that, neurons were incubated with the listed primary antibodies: β -III Tubulin (1:1000, ab78078, Abcam, Cambridge, UK), EDU (5-ethynyl-2'-deoxyuridine, E10187, ThermoFisher, MA, USA), and Cleaved Caspase 3 (1:500, ab32042, Abcam, Cambridge, UK). Next, suitable secondary antibodies and DAPI were incubated.

The spinal cord tissues were orderly perfused with saline and 4% PFA, and sliced into sections after freezing (thickness, 30 μ m). The slices were washed three times with PBS and blocked with goat serum supplemented with 3% Triton 100 for 3 h. After that, sections were incubated with the following primary antibodies: 5-HT (1:1000) (20080, ImmunoStar, WI, USA), GFAP (1:1000, ab7260, ab279290, Abcam, Cambridge, UK), NEUN (1:800) (ab177487, ab104224), CD68 (1:500, ab213323), and IBA1 (1:1000) (ab178847) purchased from Abcam (Cambridge, UK), TUNEL (11772457001, in situ cell death detection kit-POD, Roche, Basel, Switzerland), CSPGs (1:300) (C8035, Sigma-Aldrich, MO, USA), and APC (1:500) (ab16794, Abcam, Cambridge, UK). The samples were then incubated with corresponding secondary antibodies and DAPI.

For HE staining, the paraffin slices were sequentially dehydrated with 100%, 90%, 80%, and 70% alcohol for 5 min at each concentration, washed three times with PBS, stained with hematoxylin stain for 5 min, and washed with PBS. The slices were then soaked in 5% acetic acid for 1 min, washed with PBS and stained with eosin for 1 min. Finally, they were dehydrated using 70%, 80%, 90%, and 100% alcohol for 10 s at each concentration, then soaked in xylene for 1 min. The samples were then visualized by an automatic digital slide scanning system (AxioScan.Z1, Zeiss, Oberkochen, Germany). The data were analyzed by the ZEN Intellesis (Carl Zeiss Microscopy LLC, NY, USA) and image J (1.53, NIH, MD, USA) software.

Flow cytometry of primary neurons

Apoptosis and cell cycle markers of the cultured cells were evaluated by flow cytometry. For apoptosis, all cells were digested into single cells and resuspended in PBS with Annexin V-FITC/PI Apoptosis Detection Kit (KeyGEN BioTECH, Nanjing, China). After incubation at room temperature (\sim 25°C) for 10 min, the samples were tested for apoptosis using influx flow cytometers (BD Biosciences, NJ, USA). Cell cycle analysis were determined using propidium iodide (PI, sigma Aldrich, USA), and detected by flow cytometry.

Transmission Electron Microscope (TEM) analysis

Neurons samples were fixed in 1% osmium acid for 2 h, washed with PBS, and dehydrated in acetone. Next, cells were blocked in 2.5% (w/v) glutaraldehyde overnight and placed overnight in a heating polymerize at 70°C. Finally, cells were observed using TEM (Hitachi HT770, Tokyo, Japan).

Cell viability assays

3-(4,5-Dimethylthiazol-2-yl)-2,5-diphenyltetrazolium bromide (MTT, Beyotime, Shanghai, China) assays were used to evaluate cell viability. Briefly, LPS induced primary neurons were treated with BPQDs (0, 10, 50, 100, 200 and 500 μ g. mL⁻¹) for 24 h at 37°C. MTT (20 μ M, Sigma-Aldrich, USA) was added and incubated for 4 h at 37°C. Dimethyl sulfoxide (150 μ L) (Sigma-Aldrich, USA) was added to each well, and the absorbance read at 490 nm.

ELISA array for detecting bio-safety

Blood samples from rats were centrifuged for 20 min (3000 rpm), and the supernatant was collected for serum biochemical analysis, including alanine transaminase (ALT), aspartate transaminase (AST), creatinine (CREA),

Table 1. qPCR primers for key factors of rat nerve cell cycle.

| Name | Gene name | Forward (5'→3') | Reverse (5'→3') |
|-----------|-----------|------------------------|-----------------------|
| Gapdh | GAPDH | GCATCTTCTTGTGCAGTGCC | GATGGTGATGGGTTTCCCGT |
| Cyclin D1 | CCND2 | ACCTGTGAGGAAGCCATTCG | CCAGCGTGTCCCTTCTCATT |
| Cyclin D3 | CCND3 | ACACGCGTCGCTTCTCCTA | TGTGACATCTGTGGGAGTGC |
| CDK4 | CDK4 | ACCAGGATCTCCCAC TAGCA | TCAGGTCCCAGTGAACAATG |
| CDK6 | CDK6 | GGCCGCGAGTAGTCAGTTACC | CCAACACTCCAGAGGTCCAC |
| Cyclin E2 | CCNE2 | CGCAGTAGCCGTTTACAAGC | TCACTGCAAGCACCATCAGT |
| Cyclin A2 | CCNA2 | GTC AACCCCGAAAAAGTG GC | GCCTTCCATGTGTCTGACCAA |
| CDK2 | CDK2 | AGGCGGCAACATTGTTTCAA | GACAGGGACTCCAAAGGCTC |
| Cyclin B1 | CCNB1 | GGTCGATGTGGAGCAGCATA | GGCAAATGCACCATGTCGT |
| Cyclin B2 | CCNB2 | TGGCTGGTCCAAGTCCATTC | TGTGCTGCATGACTTCCAGT |
| CDK1 | CDK1 | AGGACCAGCTCACAAAAGGG | GTGGAAAAGCGGCTTCTTGG |
| P16 | CDKN2A | AACACTTTCGGTCGTACCCC | CTCCCTCCCTCTGCTAACCT |
| P21 | CDKN1A | AAGCCCGAGTTCCTGCTAAC | ATCGGCGCTTGGAGTGATAG |
| P27 | CDKN1B | GACTCACTCGCGGCTCC | TGTTTACGTCTGGCGTCGAA |

blood urea nitrogen (BUN). Fresh blood samples were used for routine blood examination to calculate white blood cell (WBC), red blood cell (RBC), hemoglobin (HGB), and platelet (PLT) levels. Detection above were performed by Servicebio (Guangzhou, China).

Protein chip and phosphorylated proteomics analysis

Total proteins from spina cord tissues (0.5 cm block of the injury center) were extracted, and homogenized in PBS with protease inhibitors, total protein concentration was adjusted to $2 \mu\text{g} \cdot \mu\text{L}^{-1}$. The protein solution was incubated with the protein chip (Proteome Profiler Rat XL Cytokine Array, ARY030, R D systems, MN, USA) according to the manufacturer's instructions. Finally, samples were detected using a chemiluminescence imaging analysis system (ImageQuant Las4000mini, Molecular Dynamics, CS, USA).

The spinal cord tissues were extracted and enzymatically hydrolyzed into peptides. Then, the phosphorylated peptides were enriched by titanium dioxide affinity chromatography and detected by mass spectrometry (TNT pro). Huada gene technology (Shenzen, China) performed the bioinformatics analysis, generated volcanic maps and other data analyses.

qPCR analysis for cell cycle

RNA isolation and the qPCR array were performed as previously described.³⁵ Briefly, the total RNA was extracted from spinal tissues (0.5 cm block of the injury center) using the TRIzol reagent (Invitrogen, MA, USA) and reverse transcribed (1 mg) to obtain cDNA using the RevertAid First-Strand cDNA Synthesis Kit (Thermo Fisher Scientific, MA, USA). The cDNA samples were analyzed using SYBR Green (Roche, Basel, Switzerland) and pre-designed primers (Sangon Biotech, Shanghai, China). GAPDH was

used as the internal control, and the relative mRNA abundance was calculated using the ΔCt method [relative mRNA abundance = $2 - (\text{Ct gene of interest} - \text{Ct GAPDH})$].³⁵ The qPCR experiments were performed in triplicate. Primers used in this study are listed in Table 1.

Western blot analysis

Spinal cord tissues were collected as described above, total protein was extracted by Cytoplasmic Protein Extraction Kit (Beyotime Biotech, Shanghai, China) and adjusted concentration to $2 \mu\text{g} \cdot \mu\text{L}^{-1}$. The protein samples were separated using gel electrophoresis, transformed onto polyvinyl membrane, and incubated with the following primary antibodies: Myc (1:1000, ab32072), Cyclin D1 (1:1000, ab16663), Bcl-xL (1:1000, ab32370), and Bcl-2 (1:1000, ab32124) from Abcam (Cambridge, UK). The bands were visualized using an enhanced chemiluminescence (ECL) western blot detection kit (Millipore, WBKLS0500, MA, USA), and analyzed using Image J (NIH, MD, USA).

Statistical analysis

The data were analyzed using GraphPad Prism 8 (GraphPad Software Inc., CA, USA). Differences between two groups were evaluated using an unpaired Student's *t*-test, while one-way ANOVA was used for multiple-group comparisons. Continuous normally distributed data were expressed as mean \pm standard deviation (SD). Statistical significance was set at $p < 0.05$.

Results

The properties of the prepared E@BP

The morphology of BPQD was observed by a transmission electron microscope (TEM). The data of TEM images showed that the BPQDs displayed excellent dispersion

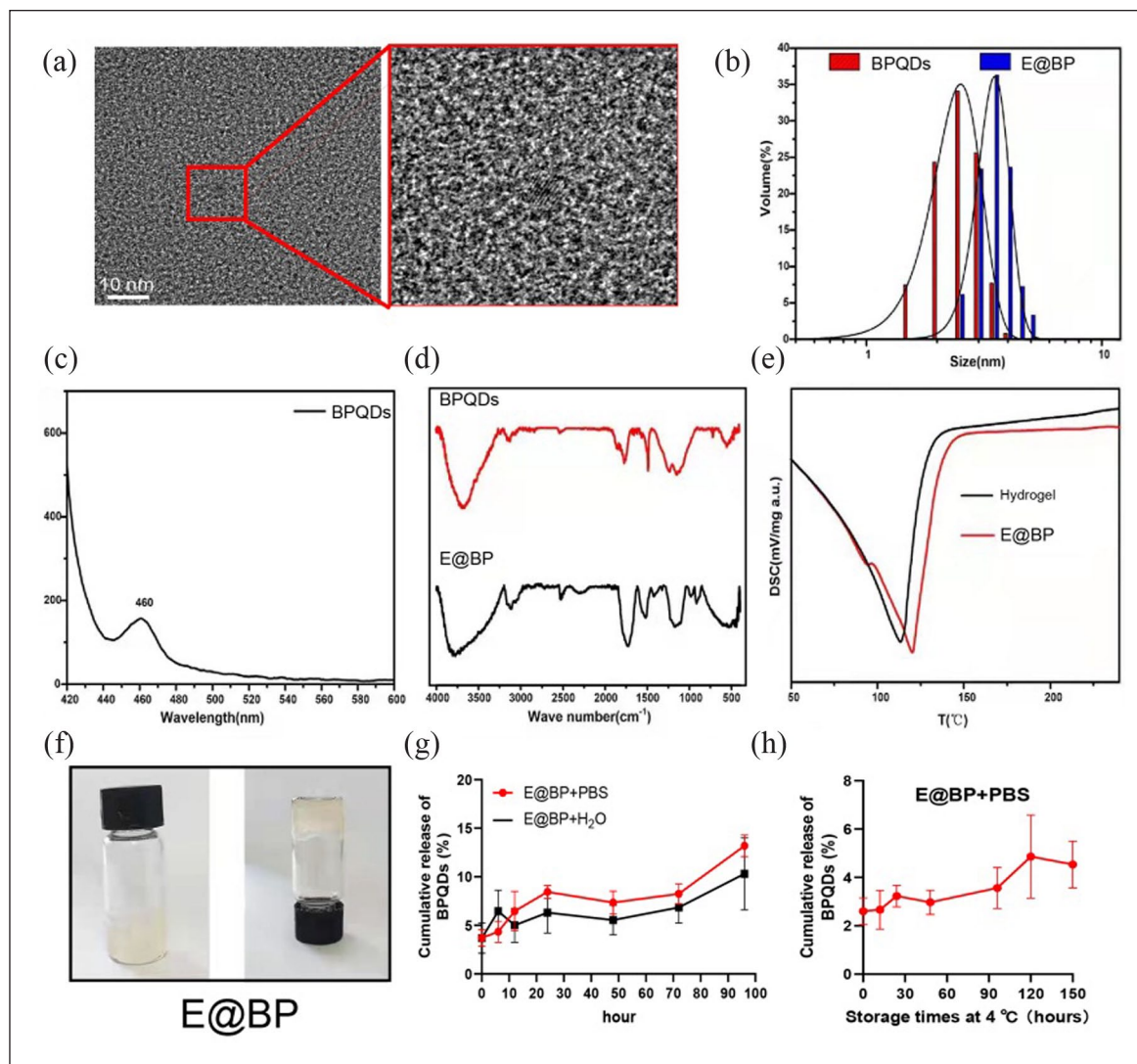


Figure 1. The characterization of E@BP. (a) TEM image of the BPQDs. The red frame shows the BPQDs under a high-resolution TEM (HRTEM). Scale: bar = 10 nm, TEM, transmission electron microscope. (b) The size of BPQDs detected by dynamic light scattering (DLS). (c) Fluorescence spectra of BPQDs. (d) Investigation of the functional groups of samples were investigated by the Fourier Transform Infrared (FTIR) Spectroscopy, 3750 cm^{-1} , represented $-\text{OH}$ bond, 1750 cm^{-1} represented $\text{C}=\text{O}$ bond, 1200 cm^{-1} characterized $\text{P}=\text{O}$ bond. (e). Thermographs of differential scanning calorimeter (DSC) analysis upon heating, both minimum values at $\sim 120^\circ\text{C}$. (f) Digital photograph of the E@BP. (g) Release profile of BPQDs encapsulated in E@BP+PBS and E@BP+ H_2O respectively. (h) After being stored at 4°C for different times, E@BP was placed in PBS to determine the release of BPQDs.

and uniformity (Figure 1(a)). Dynamic light scattering (DLS) analysis showed that the average diameters of BPQD and E@BP were approximately 3 and 3.2 nm, respectively (Figure 1(b)). The BPQDs had a sharp and strong absorption peak at about 460 nm recorded by fluorescence spectra (Figure 1(c)), which indicative of high sample quality.³⁶ The Fourier Transform Infrared (FTIR) Spectroscopy helped to investigate of the functional groups present in the material. The infrared spectrum of E@BP indicated the wide intense bands at 3750 cm^{-1} (represented $-\text{OH}$ bond) and at 1750 cm^{-1} (represented $\text{C}=\text{O}$ bond) (Figure 1(d)). Similarly, the stretching vibration at 1200 cm^{-1} was characteristic of the $\text{P}=\text{O}$ bond in

the BPQDs.³⁷ The prepared E@BP contained EGCG and BPQDs (Figure 1(d)). Thermal stability detection was carried out using differential scanning calorimetry (DSC), data showed that EGCG-hydrogel (simplified as Hydrogel) and E@BP had similar minimum values at $\sim 120^\circ\text{C}$ (Figure 1(e)). Vial Flip Test showed the E@BP were successfully prepared (Figure 1(f)). To test the stability of E@BP during treatment, the release of BPQDs in PBS (Imitated the *in vivo* microenvironment) and H_2O (Imitated the storage environment) were detected at 37°C . Release Test showed the release amount of BPQDs in PBS and H_2O were stable over time (Figure 1(g)). Indeed, to test the storage stability of E@BP, E@BP was storage

at 4, then they were taken out at different time points and placed in PBS to observe the release of BPQDs. The results showed that, short term and low temperature storage hardly affects the stability of E@BP.

Biological safety of E@BP

Rats were separated into four groups: Sham, SCI, Hydrogel, E@BP. Several assays were performed to assess the biological safety of E@BP, including serum biochemistry, routine blood parameters, HE staining and MTT. Alanine aminotransferase (ALT), aspartate aminotransferase (AST), creatinine (CREA) and blood urea nitrogen (BUN) in serum were measured by ELISA on 96 h post treatment. Data indicated that the liver functions (ALT and AST) and the renal functions (CREA and BUN) had no significant difference in the four groups (Figure 2(a)–(d)). Similarly, E@BP application did not disrupt the blood parameters, such as white blood cell (WBC), red blood cell (RBC), hemoglobin (HGB), and platelet (PLT) (Figure 2(e)–(h)). The rats were sacrificed at 8 weeks after treatments, the vital organs (heart, liver, spleen, lung, and kidney) were collected for HE staining (Figure 2(i)). Data revealed that E@BP transplantation did not induce inflammation and structural damages to the vital organs. Together, E@BP were safe for in vivo treatment. In addition, MTT assay was used to determine the cytotoxic activity of cultured LPS-injury neurons (Supplemental sFigure 1A–B). Data showed that LPS incubation decreased the viability of neurons, and E@BP treatment alleviated this damage. The optimal concentration was $100 \mu\text{g}\cdot\text{mL}^{-1}$ (100 μg BPQD in 1 mL hydrogel), the neurons were positively stained by β -III tubulin (a marker of mature neurons).

E@BP transplantation promotes the recovery of motor function in SCI rats

Rats were used to establish SCI model, and materials (Hydrogels or E@BP) were transplanted to the injury site immediately, IVIS were carried out at the first 4 days, spinal tissues were used for IHC at 56 days (Figure 3(a)). In order to detect the E@BP distribution in the SCI site, spinal cords were removed for ex vivo fluorescence images with IVIS Spectrum Imager (Figure 3(b)). Data revealed that the E@BP fluorescence intensity was highest at the T10 vertebra 24 h after treatment. It gradually decreased and weakened (detectable) at 96 h. Herein, E@BP retained at the SCI site for at least 4 days. The BBB scores and angle of the inclined plate experiments were used to observe motor function in paralyzed limbs. The BBB scores were significantly higher in the E@BP group than the SCI group from week 4 (Figure 3(c)). Similarly, the angle of the inclined plate significantly increased from 1 to 8 weeks in the E@BP than in the SCI group (Figure 3(d)). Moreover, 8 weeks after SCI, the 45° inclined climb test showed that E@

BP-treated rats used at least one hind limb to climb (Figure 3(e)). Altogether, E@BP effectively promotes the recovery of hindlimbs motor function in SCI rats.

E@BP reduce apoptosis and promote regeneration in injury neurons

Restoring the hindlimb motor function in SCI rats depends on the repair of injured neurons, which involves the regeneration and apoptosis processes. Here, primary neuronal cells of the fetal rat spinal cord were extracted for the in vitro experiments, neurons injury was stimulated by LPS incubation, and then E@BP treatment was applied (Figure 4(a)). The proportion of Caspase3 positive neurons substantially reduced in E@BP treatment group than the LPS group (Figure 4(b)). Similarly, the percentage of PI/Annexin double-positive neurons considerably decreased in the E@BP group compared with the LPS group (Figure 4(c)). TEM was used to observe the cellular ultrastructure (Figure 4(d)). Evidences of the mitochondrial morphology alteration in the LPS group were clear, such as irregular shape, edema, vacuole-like degeneration, enlargement, cistern broken. However, E@BP incubation effectively attenuated these alterations.

Next, EdU Cell Proliferation Kit were used to test the neural regeneration ability. The proportion of EDU-positive neurons was significantly increased in the E@BP group than the LPS group (Figure 4(e)). Proliferation capacity is related to the restart of cell cycle, which could be detected by flow cytometry (PI stain). The results showed that the S-to-M phase ratio of neurons significantly increased along with decreased G0 phase ratio under E@BP treatment compared with the LPS group (Figure 4(f)). This indicated that E@BP probably restart the cell cycle of the injury primary neuron. Overall, BPDQs reduce apoptosis and promote regeneration in injury primary neurons.

E@BP repairs the spinal cord tissue and reduces inflammation in SCI rats

The spinal cords were collected at week 8 for immunofluorescence staining to observe their repair efficacy. The breaks of spinal cord tissue at T10 vertebra were similar in the SCI groups and hydrogel groups that displaying obvious discontinuities on the injured sites, but E@BP transplantation alleviated the discontinuities (Figure 5(a)). 5-hydroxytryptamine (5-HT) tract is one of descending monoaminergic pathways, and have high growth capacity after injury.^{38,39} Here, 5-HT-stained axons were used to display the continuity anatomy of the spinal cord, and access the recovery of nerve fibers. The length of 5-HT positive nerve fibers significantly decreased in the SCI and hydrogel groups when compared to the E@BP group (Figure 5(b) and (c)). SCI repair is closely related to

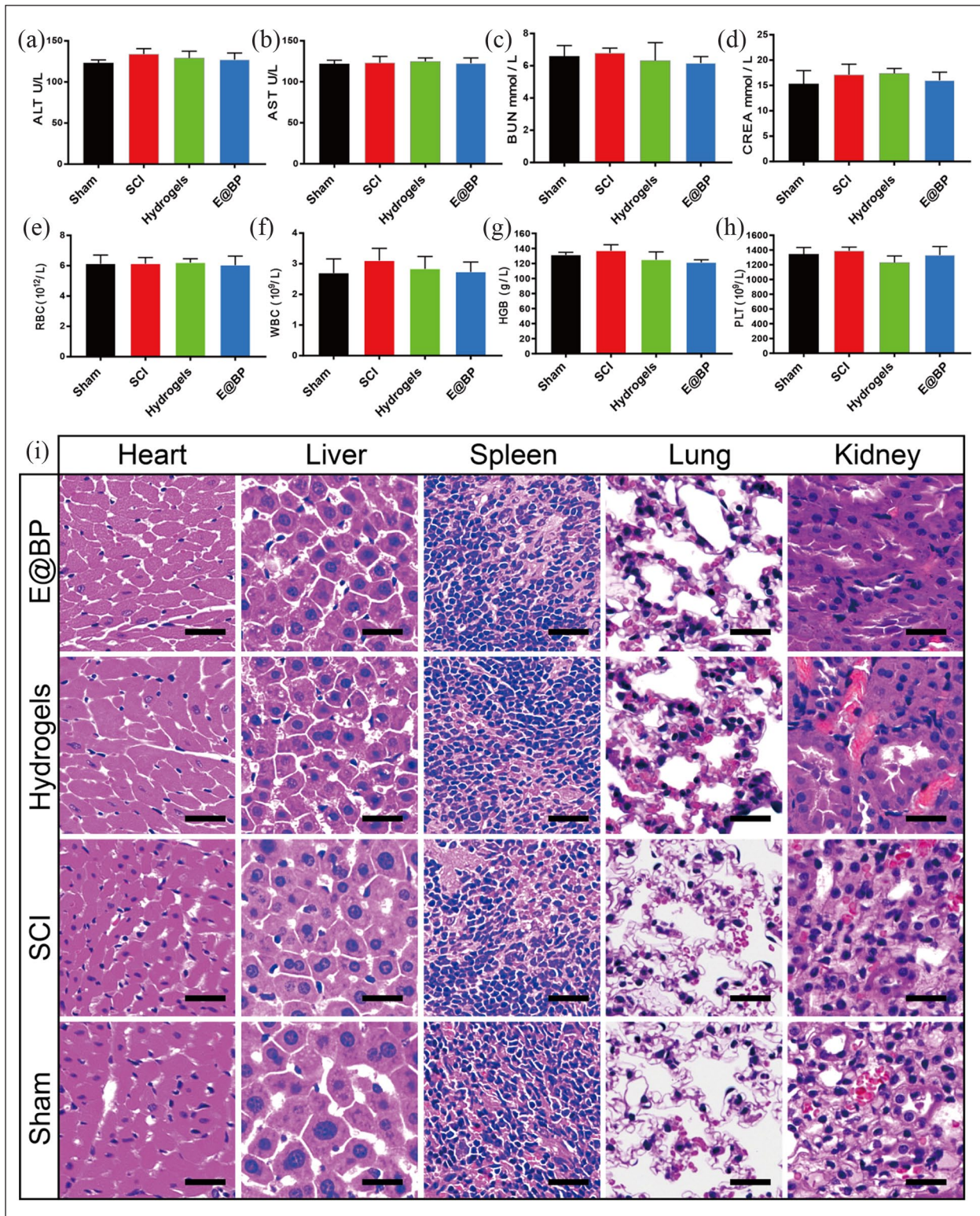


Figure 2. Biological safety evaluation in vivo. Rats were separated into four groups: Sham, SCI, Hydrogel, E@BP. (a–h) ELISA arrays of serum on 96 h post treatment to detect the expression of alanine aminotransferase (ALT), aspartate aminotransferase (AST), creatinine (CREA), blood urea nitrogen (BUN), white blood cell (WBC), red blood cell (RBC), hemoglobin (HGB), and platelet (PLT). The experiments were performed in triplicate. $**p < 0.01$, $***p < 0.001$, $N p > 0.5$. (i) Representative images of HE staining of the vital organs (heart, liver, spleen, lung, and renal) from the rats 8 weeks post treatment. Scale: 1 bar = 100 μm, $n = 3$.

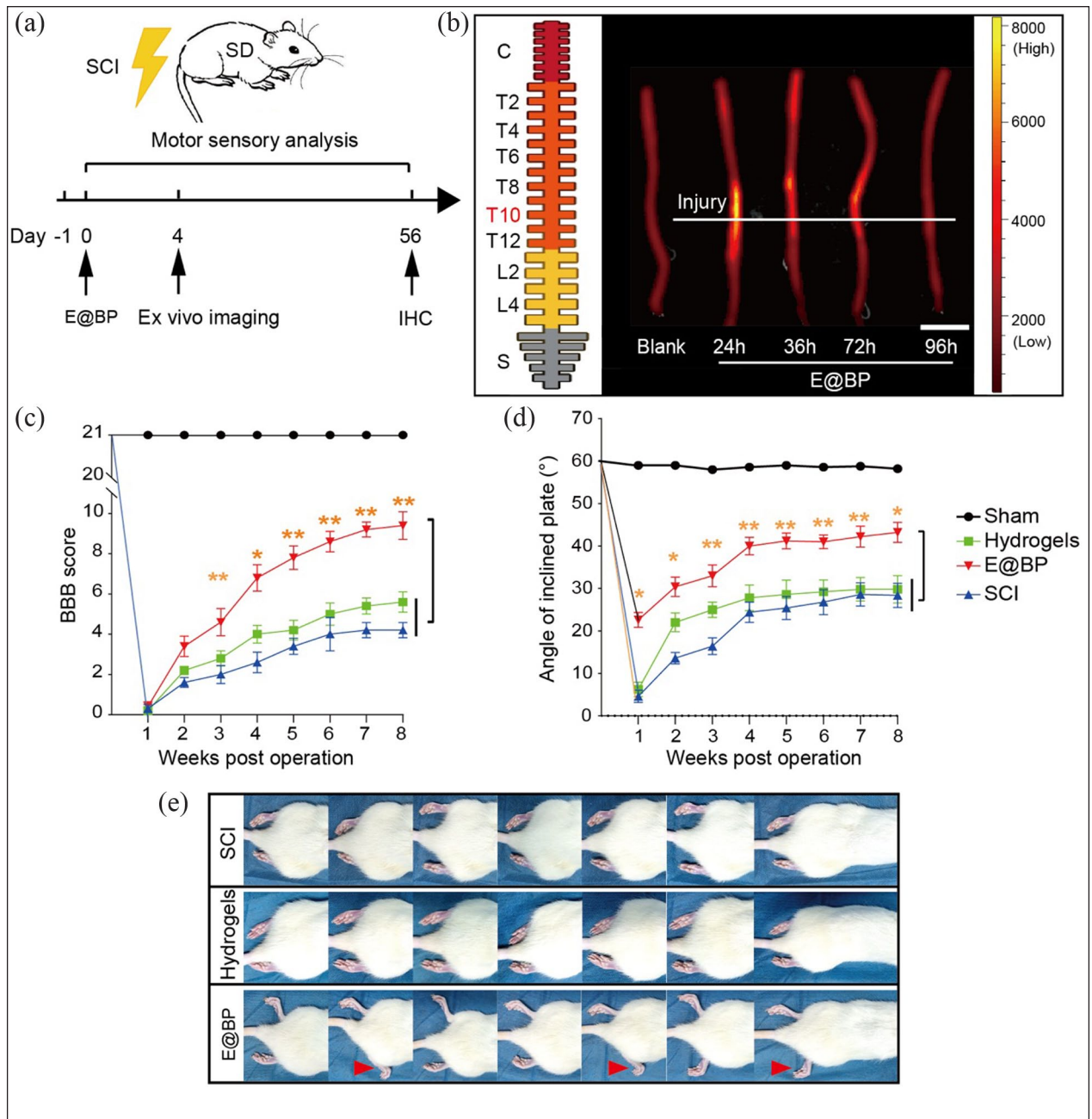


Figure 3. E@BP transplantation promotes the recovery of motor function in SCI rats. (a) Scheme of experimental procedure. (b). Ex vivo fluorescence images of the spinal cord tissues detected by *IVIS Spectrum Imager*. Blank is the control group without E@BP treatment. 24, 36, 72, and 96 h represent different time points after E@BP treatment. (c) BBB scores of rats from different groups. *E@BP versus SCI, * $p < 0.05$, ** $p < 0.01$, $n = 7$. (d) Statistical analysis of inclined plane test in each group of rats. *E@BP versus SCI, * $p < 0.05$, ** $p < 0.01$, $n = 7$. (e). Motor function of hind limbs in SCI model rats at 8 weeks. The red arrow indicates the bending movement of the ankle of the hind limb.

neuron survival and astrocyte accumulation in the injured area, which could be observed by NEUN and GFAP immunofluorescence staining, respectively (Figure 5(d)). The GFAP positive area ratio significantly decreased in the injured spinal cords of the SCI groups and hydrogels groups than the E@BP group (Figure 5(e)). Accordingly, the percentage of NEUN-positive cells per HPF in the

injured area was lower in the SCI and hydrogel groups than the E@BP group (Figure 5(f)).

Chondroitin sulfate glycoproteins (CSPGs) is one of the key inhibitors to nerve regeneration after SCI, which secreted by reactive astrocytes. We measured the CSPGs expression of the injured tissue at 8 weeks post-SCI. The results showed that CSPGs density significantly

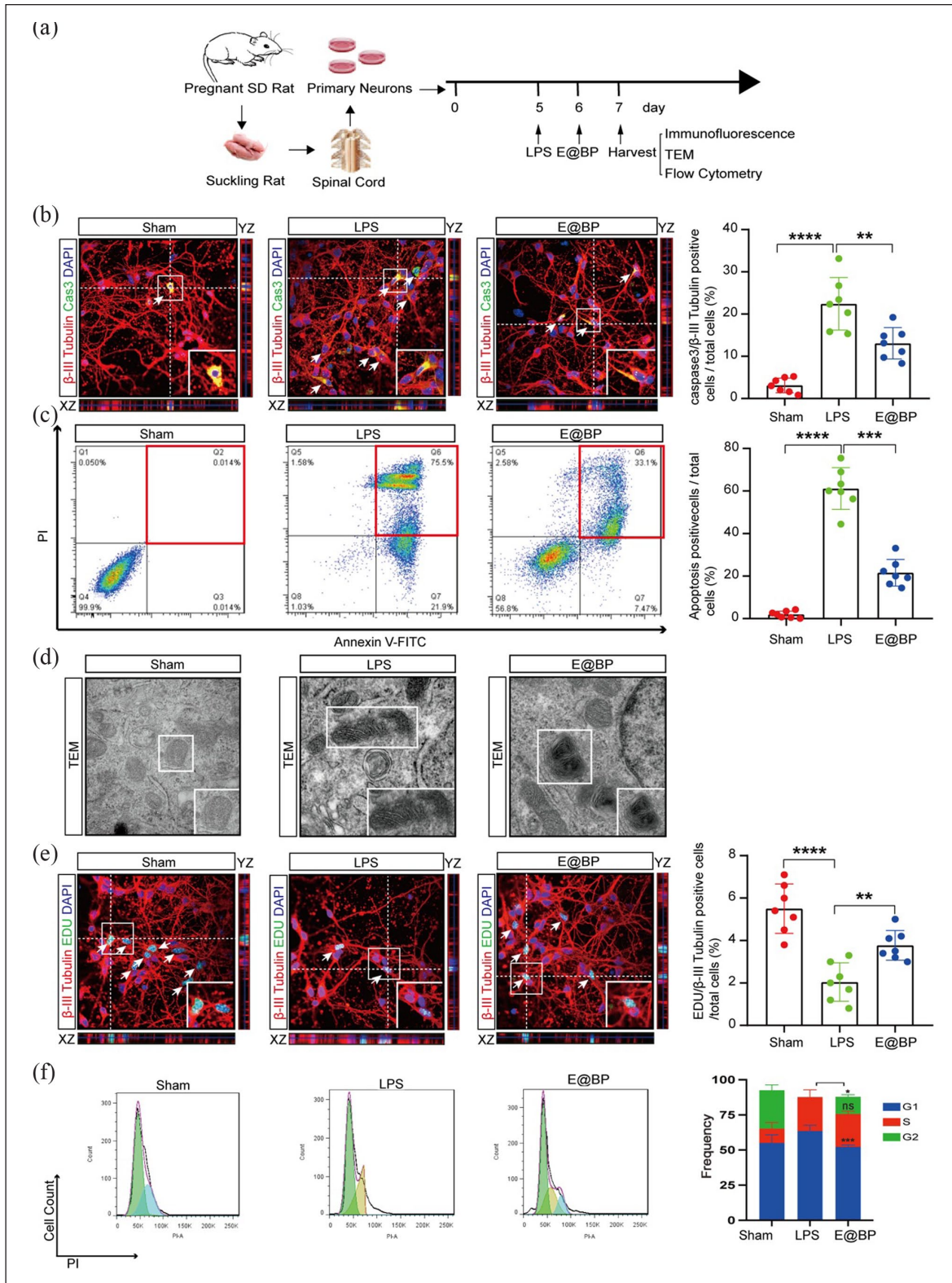


Figure 4. E@BPP reduce apoptosis and promote regeneration in injury neurons. (a) Scheme of experimental procedure. (b). Confocal images of β -III-Tubulin (red) and Cleaved-Caspase-3 (green), Dapi (blue). White arrows represent double-positive cells. $**p < 0.01$, $****p < 0.0001$, $n = 7$, bar = 100 μm . (c). Flow cytometric detection of apoptosis. The red box represents PI and annexin double-positive cells. $**p < 0.01$, $****p < 0.0001$, $n = 7$. (d). Transmission electron microscope (TEM). White boxes pointed out mitochondria, bar = 50 nm. (e). Confocal image of β -III-Tubulin (red) and EDU (green), Dapi (blue). White arrows represent double-positive cells. $**p < 0.01$, $****p < 0.0001$, $n = 7$, bar = 100 μm . (f). Flow cytometric detection of the cell cycle. $n = 3$.

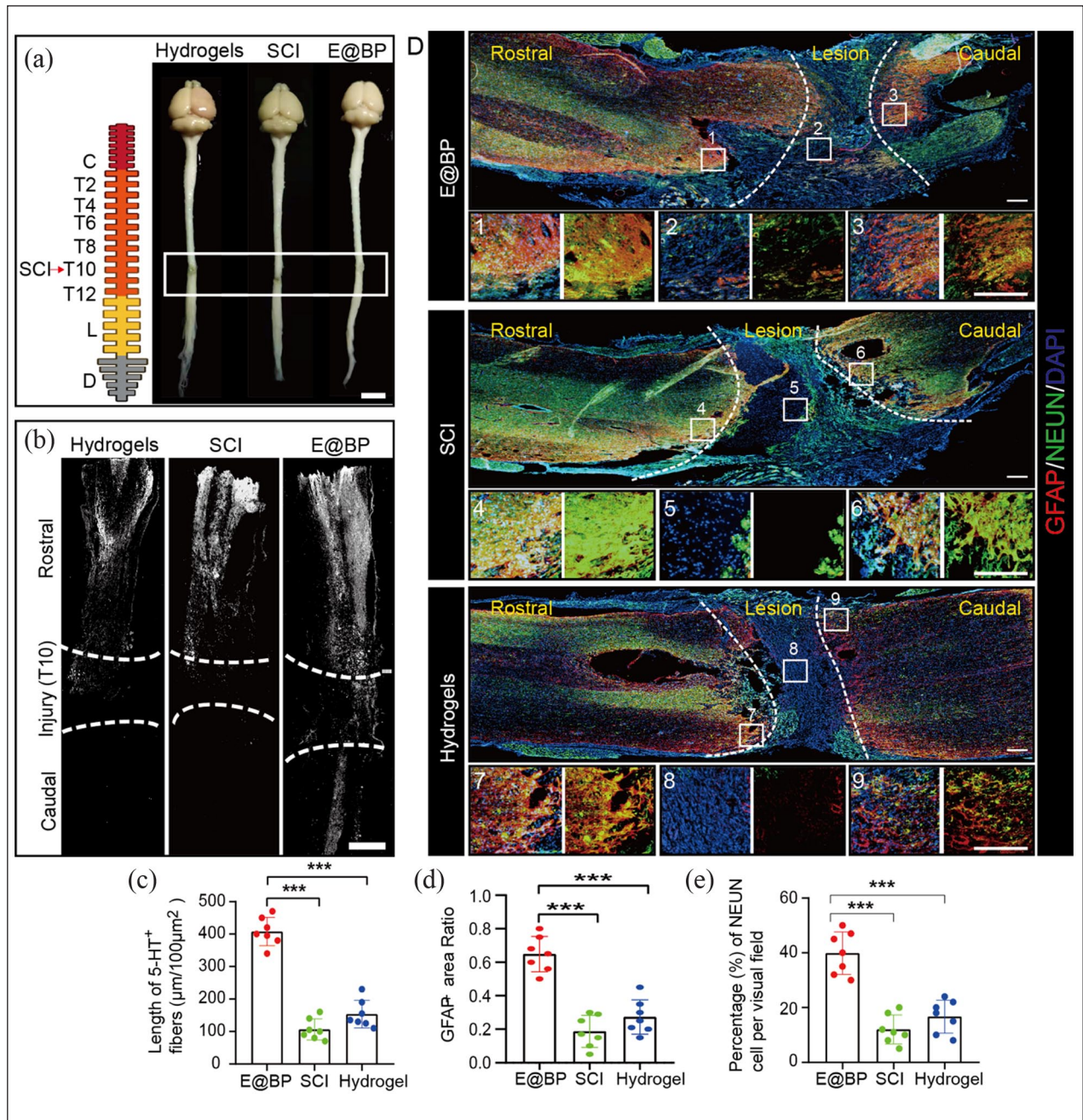


Figure 5. E@BP repairs the spinal cord tissue in SCI rats. (a) Representative gross specimens of spinal cords, scale bar = 1 cm. (b and c) Confocal images and statistical analysis of 5-HT (white) staining. *** $p < 0.001$, $n = 7$, bar = 200 μm . (d-f) Confocal images and statistical analysis of GFAP (red) and NEUN (green), the white boxes are enlarged to show the details with or without DAPI display, respectively, GFAP area Ratio indicated area occupied by GFAP positive stained per high-power field. *** $p < 0.001$, $n = 7$, bar = 200 μm .

decreased in E@BP groups compared to SCI groups and hydrogel groups (Supplemental sFigure 2 A-B). Oligodendrocytes participate to form the axon myelin sheath in CNS, and function to nourish axons. Anti-adenomatous polyposis coli (APC) is most commonly used to specifically label the cell bodies of mature oligodendrocytes. Apoptosis of oligodendrocytes obviously

causes spinal cord demyelination, which impeding SCI repair. Indeed, the apoptotic oligodendrocytes (TUNEL positive APC) in the injured sites greatly reduced under E@BP intervention when compared with SCI and hydrogels rats (Supplemental sFigure 2C-D). Collectively, these evidences elucidated that E@BP repairs the spinal cord tissue in SCI rats.

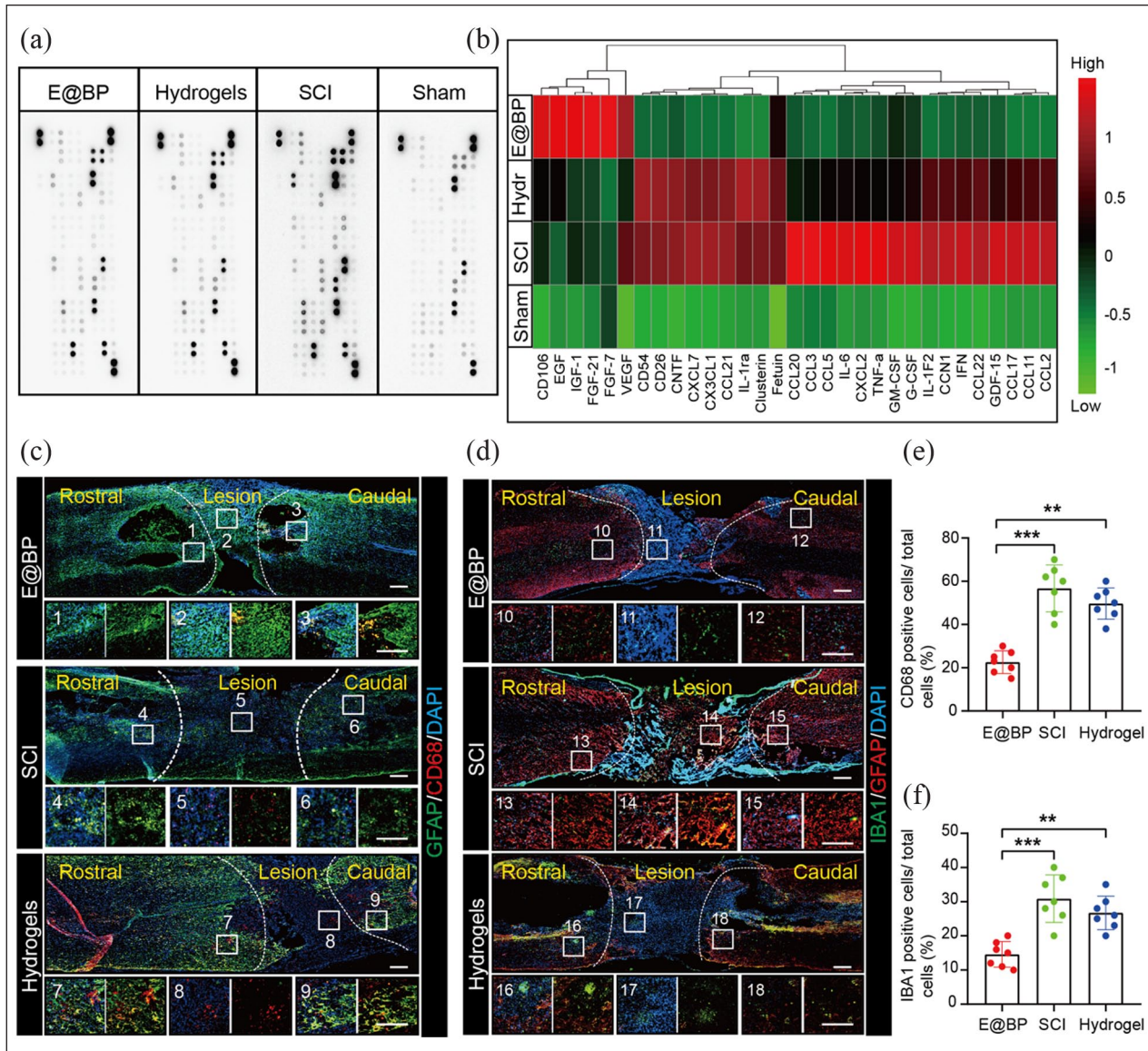


Figure 6. E@BP reduces inflammation in SCI rats. (a and b). Protein chip images and data to investigate inflammation. $n = 3$. (c and e). Confocal images and statistical analysis of CD68 (red) and GFAP (green), the white boxes are enlarged to show the details with or without DAPI display, respectively. ** $p < 0.01$, *** $p < 0.001$, $n = 7$, bar = 200 μm . (d and f). Confocal images and statistical analysis of GFAP (red) and IBA1 (green), the white boxes are enlarged to show the details with or without DAPI display, respectively. ** $p < 0.01$, *** $p < 0.001$, $n = 7$, bar = 200 μm .

E@BP reduces inflammation in SCI rats

Inflammation is another key impediment to repair spinal cord after SCI. To verify post-SCI inflammation and repair, spinal cord tissue was harvested at 2 weeks post SCI and was tested using a protein chip (Figure 6(a)). All significantly changed proteins were used to draw the heat map, which elucidated their expression profiles (Figure 6(b)). In detail, five repair-related factors (CD106, EGF, IGF-1, FGF, and VEGF) significantly increased in the E@BP groups than the SCI and hydrogel groups. The inflammation-inducing factors (CD54 and CD26) significantly reduced in the E@BP group. Correspondingly, pro-inflammatory cytokines and chemokines (IL-1, TNF- α , CCL3, CCL5, and CCL11) significantly

decreased in the E@BP groups than the SCI and hydrogel groups. Interestingly, macrophage chemotactic factors (CCL2, CCL3, CCL5, CCL17, and CCL22) significantly reduced after E@BP therapy. These data suggested that anti-inflammatory effect of E@BP may be coupled to inhibit macrophage and microglia activation. CD68 and IBA1 signals indicates microglia. Spinal cord tissues were harvested at 2 weeks post treatment, observed by CD68 and IBA1 immunofluorescence staining. The results showed that E@BP both decreased the number of CD68 positive and IBA1 positive cells in the injured area (Figure 6(c)–(f)). Collectively, E@BP reduces inflammation, especially inhibits the activation of macrophage and microglia at injured spinal cord of SCI rats.

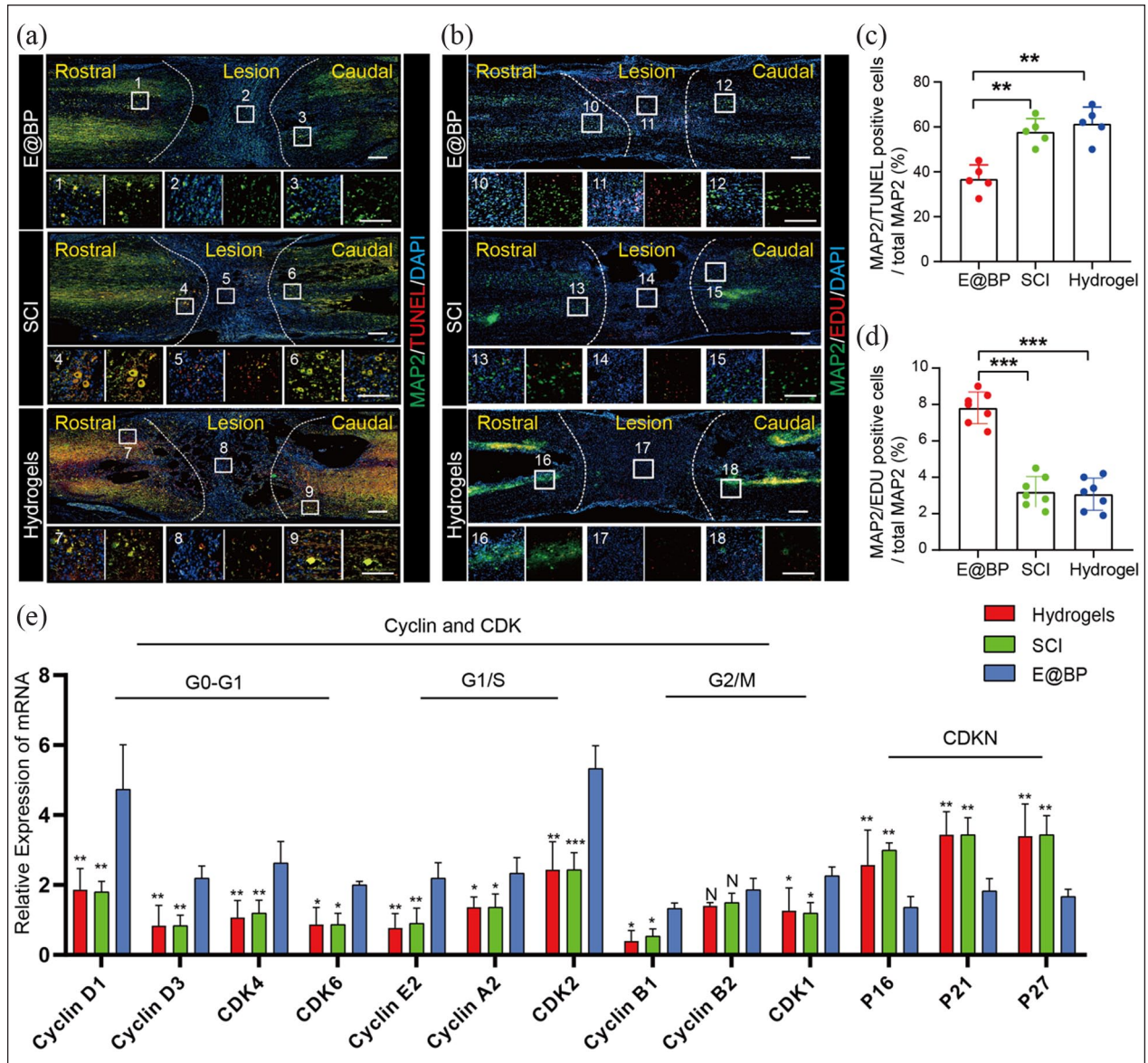


Figure 7. E@BP reduces neuronal apoptosis and promotes neuronal regeneration in SCI rats. (a and c). Confocal images and statistical analysis of TUNEL (red) and MAP2 (green), the white boxes are enlarged to show the details with or without DAPI display, respectively. $**p < 0.01$, $n = 7$, bar = 200 μm . (b and d). Confocal images and statistical analysis of EDU (proliferation, red) and MAP2 (neuronal marker, green), the white boxes are enlarged to show the details with or without DAPI display, respectively. $***p < 0.001$, $****p < 0.0001$, $n = 7$, bar = 200 μm . (e). qPCR detection of key cell cycle related factors of primary neurons. N: the difference was statistically insignificant, $*p < 0.05$, $**p < 0.01$, $***p < 0.001$, $n = 3$.

E@BP reduces neuronal apoptosis and promotes neuronal regeneration in SCI rats

Balance of apoptosis and proliferation determined tissues' homeostasis, especially in neural fate with spinal cord damages. The level of neural apoptosis and regeneration was detected at 5 weeks post SCI using immunofluorescence, MAP2 serves as a neuronal marker here (Figure 7(a) and (b)). Data statistic showed that TUNEL-positive neurons significantly decreased in the E@BP groups (Figure 7(c)). EDU-positive neurons obviously increased in the E@BP

groups compared to SCI and hydrogel groups (Figure 7(d)). We focused on further exploration of proliferation by qPCR analyzing gene expression related to cell cycle of primary neurons. As expected, E@BP significantly enhanced expression of stimulating factors (cyclin and CDK family), and reduced the cell cycle inhibitors (CDKN family) than the other two groups (Figure 7(e)). This process facilitated the transition of neuron from quiescent state into division. Collectively, E@BP inhibits neuronal apoptosis after SCI, and enhances neuronal regeneration by regulating the gene expression associated to cell cycle.

The molecular mechanism of E@BP repairs spinal cord in SCI rats

Phosphorylation proteomics were used to explore the underlying molecular mechanism of E@BP on spinal cords 1 week after SCI in regulating post translational modification (Figure 8(a)). The results showed that E@BP massive increased the phosphorylation of proteins, mainly involving serine (S) and glutamic (E) acid (Figure 8(b) and (c)). The phosphorylated proteins participated in spinal cord development and inhibited the apoptosis of neurons (Figure 8(d)). Indeed, the differentially phosphorylated proteins for spinal cord development and neural apoptosis were enriched in the AKT signaling pathway (Figure 8(e)). The phosphorylation of PDK1, AKT, GSK3, 14-3-3, and BAD was higher in the E@BP group than in the SCI groups (Supplemental sFigure 4). Other phosphorylated peptides in the AKT pathway are shown in Supplemental sFigure 3. Myc and Cyclin D1 are cell cycle promoting factors, served as downstream proteins of the PDK1/AKT/GSK3 pathway. BCL-XL and BCL-2 are apoptosis inhibitory protein, represented as downstream proteins of the PDK1/AKT/14-3-3/BAD pathway. Data from western blot proved that the expression of Myc, Cyclin D1, BCL-XL, BCL-2 were higher in the E@BP group than SCI and Hydrogels groups (Figure 8(f) and (g)). Altogether, E@BP may regulate the PDK1/AKT/GSK3 pathway promoting cell cycle progression, and mediate the PDK1/AKT/14-3-3/BAD pathway to reduce apoptosis in SCI rats (Figure 8(h)).

Discussion

In this study, E@BP was prepared and verified its role in repairing neurons after SCI in rats. E@BP showed good biocompatibility and stability. E@BP promoted the proliferation of the primary neural cells from embryo spinal cords. E@BP promoted the structural integrity and functional recovery in the SCI rats. In addition, E@BP reduced inflammation responses and promoted neural regeneration in the injury sites. These therapeutic effects of E@BP probably relate to regulate the phosphorylation of key proteins in the AKT signaling pathway.

SCI is characterized by significant motor and sensory nerve dysfunction that occurs below the injured nerve segment, often causing lower-limb paralysis.⁴⁰ Injury of superior neurons interrupts nerve conduction, which resulting in inactivating effector organs.¹³ E@BP promoted the recovery of motor nerve function after SCI in vivo. Neurons play an essential role in propagating electrical signals through the spinal cord, such as forming nerve conduction bundles and regulating the function of target organs.⁴¹ Therefore, repairing neurons is critical. In our study, E@BP incubation could attenuate apoptosis and increase proliferation of primary neurons. Also, the enhancement of proliferative capacity might be related to activation of cell cycle. These functions guaranteed

neuronal number during the repair process. TEM images of mitochondrial morphology in primary neurons suggest that E@BP confers mitochondrial morphological stability. Mitochondria morphology closely associated with cellular state. Sun et al. reported that swelling mitochondria is related to common forms of programmed cell death (apoptosis).⁴² Also, Rintoul et al. found that alteration of mitochondrial morphology in neuron affected cellular movement ability, which is vital to maintain neuronal viability and synaptic activity.⁴³ The results of this study indicate the E@BP promoted neuronal regeneration of native neurons via restarting of the cell cycle, leading to proliferation and replacement of apoptotic neurons.

The primary injury of SCI is caused by the initial trauma, and results in multiple secondary damage cascades. Hellenbrand et al. reviewed that inflammation following SCI is a complex process that involve multiple cell types.⁴⁴ Microglia, the resident immune cells, quickly respond to SCI injury to protect spinal cord. And then, they rapidly change to proinflammatory cells and release cytokine to attract glia, such as astrocytes, oligodendrocytes. Astrocytes respond to inflammatory signals within 30-min post-injury, and can themselves promote inflammation.⁴⁵ Reactive astrocytes proliferation contributes to the inhibitory microenvironment of CNS injury and potentiates secondary injury mechanisms, such as inflammation, oxidative stress, and glutamate excitotoxicity, which facilitate neurodegeneration.⁴⁶ Furthermore, strongly reactive astrocytes in the scar display clusters of GLAST and GLT-1 immunoreactivity and impaired glutamate transport activity.⁴⁷ Hara et al. reported that reactive astrocytes interacted with type I collagen to induce astrocytic scar formation through the integrin-N-cadherin pathway after SCI.⁴⁸ The stiffening abnormal scar tissues constrict the injured area and obstruct nerve conduction bundles from transducing signals, impedes continuous repairing of injured spinal cord.⁴⁹ Woods et al. considered that stiffness and composition within scaffold environments play an essential role in the release of pro- or anti-inflammatory astrocyte markers. They designed a collagen-IV and fibronectin biomimetic scaffold to optimally induce morphological features typical of quiescent astrocytes.⁵⁰ Microglia also release proinflammatory cytokines and neurotoxic agents such as free radicals and glutamate post SCI. Hence, both astrocytes and microglia are responsible for secondary neuronal death following SCI. In our study, E@BP reduced the accumulation of astrocytes, macrophages and microglia in the injured area. In detail, E@BP effectively reduced the level of pro-inflammatory factors and inhibited macrophage-related chemokines. In addition, the extensively activated astrocytes in the injury epicenter secreted CSPGs after SCI.⁵¹ CSPGs along with astrocytes mainly form glial scar, and act as a physical barrier to impede axon regrowth after spinal cord injury.⁵² CSPGs was also identified as a nonpermissive substrate for oligodendrocytes, which impede remyelination and result to poor healing.^{53,54}

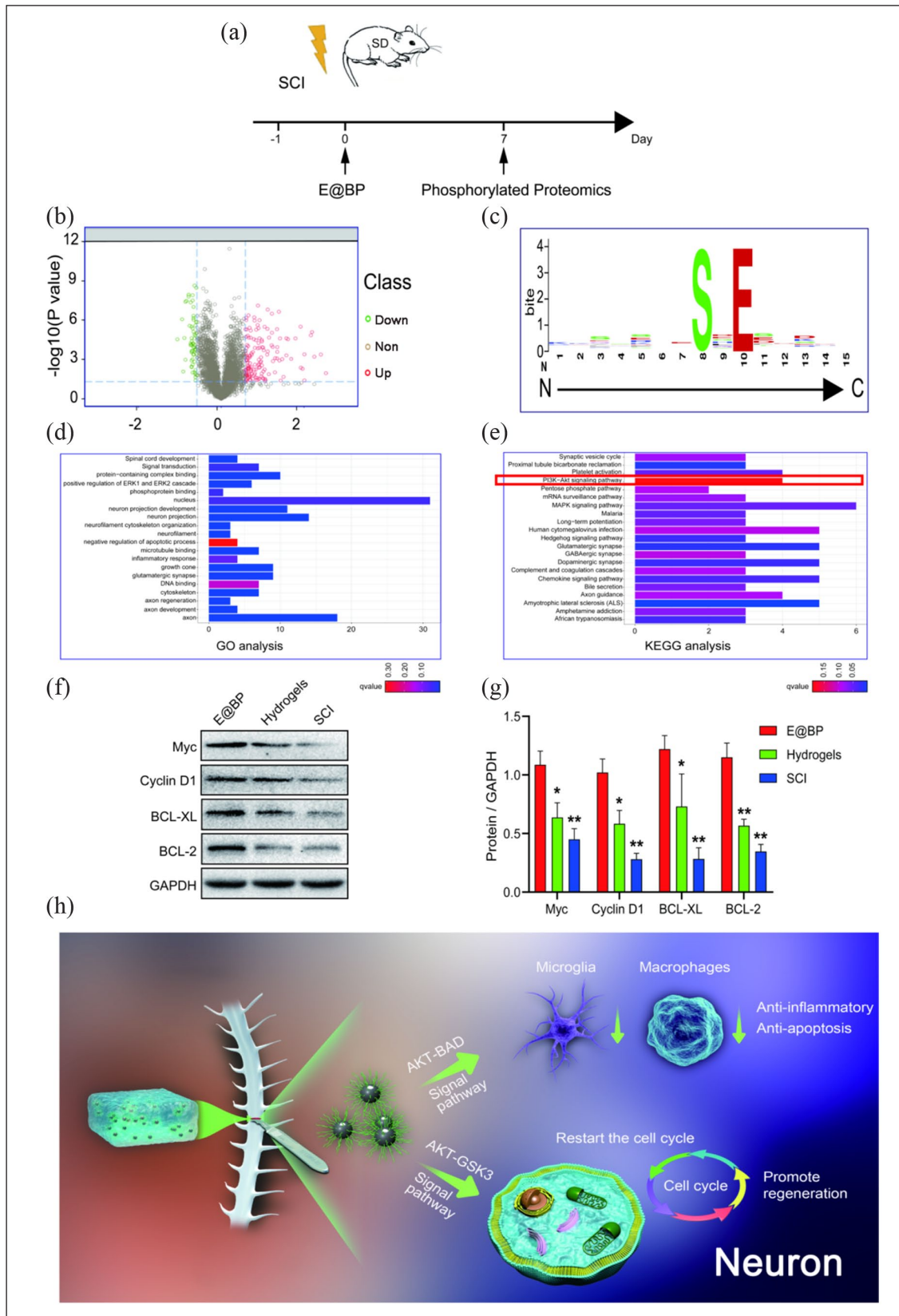


Figure 8. The molecular mechanism of E@BP repairs spinal cord in SCI rats. (a) Scheme of experimental procedure. (b) Volcano map (E@BP vs SCI). (c) Motif map (E@BP vs SCI). (d) GO analysis (E@BP vs SCI). (e) KEGG analysis (E@BP vs SCI). The red box is the most enriched signal pathway with the most phosphorylated peptides. (f and g). Western blot detection. (h). Pattern diagram. * $p < 0.05$, ** $p < 0.01$, $n = 3$.

In our study, E@BP effectively reduced CSPGs. CSPGs are also major components of the extracellular matrix sheath and perineuronal nets.⁵⁵ Wallerian degeneration occurs following SCI, characterized by axonal degeneration, myelin loss, astrocytic activation and CSPG expression.⁵⁶ Hence, we accordingly hypothesized that E@BP might also reduce Wallerian degeneration and axonal demyelination to attenuated axonal retraction.

Normally, oligodendrocytes, as a type of glial cell, provide support and insulation to CNS axons by creating and maintaining the myelin sheath.⁵⁷ oligodendrocytes loss resulting from SCI would contribute to demyelination.⁵⁸ Also, inflammatory events post SCI could cause oligodendrocytes death and demyelination.⁵⁹ Gensel et al. reported that dectin-1 activation causes macrophage-mediated demyelination and axonal injury.⁶⁰ Thus, protecting oligodendrocytes is important for stabilizing the myelin and neurons. In this study, E@BP effectively reduced apoptosis of oligodendrocytes in SCI model rats. As shown in the changes of immune-cytokine expression, immunohistochemistry of cell-specific markers, E@BP modulated the inflammatory behavior of astrocytes, macrophage and microglia. Yet, there are some anti-inflammatory treatments for spinal cord repair, such as drugs, drug loaded particles and immunomodulatory materials. In clinical, high-dose methylprednisolone drug (corticosteroids) is used for acute spinal cord injury patients to inhibit inflammation, but it could not contribute to better neurologic recoveries and may increase the risk of adverse events.⁶ Ma et al. have designed a GDNF-Loaded polydopamine nanoparticles-based anisotropic scaffolds and used to promote spinal cord repair through scavenging ROS and promoting microglia M2 polarization.⁶¹ In Shen et al.'s research, they designed an immunoregulatory hydrogel scaffold functioned to release IL-10 and scavenge damage-associated molecular patterns, which suppressed proinflammatory cytokine production and promoted the M2 macrophage/microglia phenotype in SCI mouse.⁶² In our study, E@BP have multiple functions to repair the spinal cords, including reduction of inflammatory factors, regulation of astrocytes and oligodendrocytes as well as protecting neurons and promoting their proliferation.

The inflammatory response post SCI can arrest the cell cycle of neurons and induce neuronal apoptosis.⁶³ Phosphorylation is an essential component of cell physiology and plays a key role in regulating the cell cycle.⁶⁴ Studies have shown that BPQDs strongly promote the phosphorylation of tissue cells and can add phosphate groups to proteins.⁶⁵ In this study, E@BP activates the cell cycle-promoting factors and reduces the inhibiting modulators, indicating that E@BP can promote neuronal regeneration by restarting cell cycle. E@BP activates the AKT signaling pathway by promoting the phosphorylation of key proteins. Particularly, E@BP promoted the phosphorylation of PDK1, AKT, and GSK3, which increased the expression of cell cycle-promoting factors (Myc and cyclin D1). Moreover, E@BP promotes

14-3-3 and BAD phosphorylation to dissociate BAD from the apoptotic complex, protecting neurons from apoptosis. According to the proteomics data (Figure 8(d) and (e)), mitogen-activated protein kinases (MAPK) families were mostly upregulated in the KEGG analysis (Figure 8(e)). Extracellular signal-regulated kinase (ERK) is one important subfamily of MAPK, which also upregulated in GO analysis (Figure 8(d)). MAPK families play an important role in proliferation and development programs by regulation of cell cycle engine and other cell proliferation related proteins.⁶⁶ Franco et al. reviewed that MAPK were modulated by G-protein-coupled receptors to impact neuroprotection and cognition in Alzheimer's disease.⁶⁷ In addition, Hu et al. established a thermosensitive heparin-poloxamer hydrogel encapsulated bFGF and NGF to treat SCI, the underlying neuroprotective and regenerative mechanism were likely through activating PI3K/Akt and MAPK/ERK signaling pathways.⁶⁸ For E@BP therapy, MAPK/ERK may be another potential pathway to repair SCI.

There are several limitations of the study that are important to consider. Firstly, the retention time of E@BP in the injury site were no more than a week after transplantation. Nevertheless, this is roughly coincided with the expectations of exerting efficacy at the early stage (acute phase). Secondly, we only observed the morphology and partial function of the major organs to assess risks. Distant potential risks are uncertain. Furthermore, BBB score and inclined plane test were used to evaluate hindlimb motor function after SCI, and sensory function was not assessed. The therapeutic efficacy of E@BP was accessed by comparing with non-activity constituents and injury controls, but not the reported novel treatment (e.g. drug loaded particles and immunomodulatory hydrogels). Moreover, E@BP is a broad pro-phosphorylation material, although it has a well-established role in reparative profile, but the potential of off-targets effects is not investigated. Finally, E@BP was used to treat spinal cord in this study, its function to cerebral injury were not clear. Considering both spinal cord and brain were part of CNS, E@BP acting on brain is worth investigation. The therapeutic efficacy of E@BP was assessed by comparing with non-activity constituents and injury controls, but not compared with other novel scaffolds in the next experiments.

Conclusion

In summary, E@BP exhibits good biological performance. E@BP inhibits inflammation at the SCI microenvironment and promotes neural regeneration, which probably relates to the phosphorylation and activation of the AKT signaling pathway. E@BP is a promising treatment option for SCI repair.

Acknowledgements

Thanks to the Guangdong Medical Laboratory Animal Center.

Author contributions

Yuanlong Li and Dong-Mei Xie: conceptualized this study, designed the methodology, performed the majority of experiments, and wrote the original manuscript draft. Qingqiang Tu: analyzed the data. Chuanwei Sun and Suyi Li: designed the methodology and searched for Resources. Xifan Mei and Yu Zhang: Resources, reviewed and edited the manuscript, sourced for funding.

Declaration of conflicting interests

The author(s) declared no potential conflicts of interest with respect to the research, authorship, and/or publication of this article.

Funding

The author(s) disclosed receipt of the following financial support for the research, authorship, and/or publication of this article: This work was supported by the High-level Hospital Construction Project (KJ012019100), the China Postdoctoral Science Foundation (2022m720037), the Guangdong Natural Science Foundation (2022A1515111087), Guangdong Provincial Medical Research Fund (KY-Z-2022-294).

Ethics approval and consent to participate

The study was approved by the Ethics Committee of Guangdong Provincial People's Hospital.

ORCID iDs

Dong-Mei Xie  <https://orcid.org/0000-0001-8222-6369>

Yuanlong Li  <https://orcid.org/0000-0003-0387-1904>

Supplemental material

Supplemental material for this article is available online.

Data availability statement

The data that supports the findings could be provided by the corresponding author on reasonable request.

References

- Holmes D. Spinal-cord injury: spurring regrowth. *Nature* 2017; 552: S49.
- Li HL, Xu H, Li YL, et al. Epidemiology of traumatic spinal cord injury in Tianjin, China: an 18-year retrospective study of 735 cases. *J Spinal Cord Med* 2019; 42: 778–785.
- Li J, Liu G, Zheng Y, et al. The epidemiological survey of acute traumatic spinal cord injury (ATSCI) of 2002 in Beijing municipality. *Spinal Cord* 2011; 49: 777–782.
- Yang R, Guo L, Huang L, et al. Epidemiological characteristics of traumatic spinal cord injury in Guangdong, China. *Spine* 2017; 42: E555–E561.
- Rouanet C, Reges D, Rocha E, et al. Traumatic spinal cord injury: current concepts and treatment update. *Arg Neuropsiquiatr* 2017; 75: 387–393.
- Liu Z, Yang Y, He L, et al. High-dose methylprednisolone for acute traumatic spinal cord injury: A meta-analysis. *Neurology* 2019; 93: e841–e850.
- Choi SH, Sung CH, Heo DR, et al. Incidence of acute spinal cord injury and associated complications of methylprednisolone therapy: a national population-based study in South Korea. *Spinal Cord* 2020; 58: 232–237.
- Li Y, Guo Y, Fan Y, et al. Melatonin enhances autophagy and reduces apoptosis to promote locomotor recovery in spinal cord injury via the PI3K/AKT/mTOR signaling pathway. *Neurochem Res* 2019; 44: 2007–2019.
- Li Y, Lin S, Xu C, et al. Triggering of autophagy by baicalin in response to apoptosis after spinal cord injury: possible involvement of the PI3K activation. *Biol Pharm Bull* 2018; 41: 478–486.
- Fan Y, Li Y, Huang S, et al. Resveratrol-primed exosomes strongly promote the recovery of motor function in SCI rats by activating autophagy and inhibiting apoptosis via the PI3K signaling pathway. *Neurosci Lett* 2020; 736: 135262.
- O'Shea TM, Burda JE and Sofroniew MV. Cell biology of spinal cord injury and repair. *J Clin Invest* 2017; 127: 3259–3270.
- Madabhushi R, Pan L and Tsai LH. DNA damage and its links to neurodegeneration. *Neuron* 2014; 83: 266–282.
- Fan B, Wei Z, Yao X, et al. Microenvironment imbalance of spinal cord injury. *Cell Transplant* 2018; 27: 853–866.
- Gensel JC and Zhang B. Macrophage activation and its role in repair and pathology after spinal cord injury. *Brain Res* 2015; 1619: 1–11.
- Orr MB and Gensel JC. Spinal cord injury scarring and inflammation: therapies targeting glial and inflammatory responses. *Neurother* 2018; 15: 541–553.
- Zhang Y, Zhang L, Shen J, et al. Two-photon-excited fluorescence microscopy as a tool to investigate the efficacy of methylprednisolone in a mouse spinal cord injury model. *Spine* 2014; 39: E493–E499.
- Zou W, Yang S, Zhang T, et al. Hypoxia enhances glucocorticoid-induced apoptosis and cell cycle arrest via the PI3K/Akt signaling pathway in osteoblastic cells. *J Bone Miner Metab* 2015; 33: 615–624.
- Li S, Zeng M, Yang L, et al. EDNRB reverses methylprednisolone-mediated decrease in neural progenitor cell viability via regulating PI3K/Akt pathway and lncRNA expression. *J Mol Neurosci* 2020; 70: 403–412.
- Ye J, Qin Y, Tang Y, et al. Methylprednisolone inhibits the proliferation of endogenous neural stem cells in nonhuman primates with spinal cord injury. *J Neurosurg Spine* 2018; 29: 199–207.
- Schröter A, Lustenberger RM, Obermair FJ, et al. High-dose corticosteroids after spinal cord injury reduce neural progenitor cell proliferation. *Neuroscience* 2009; 161: 753–763.
- Huang S, Xu S, Hu Y, et al. Preparation of NIR-responsive, ROS-generating and antibacterial black phosphorus quantum dots for promoting the MRSA-infected wound healing in diabetic rats. *Acta Biomater* 2022; 137: 199–217.
- Xu S, Chang L, Hu Y, et al. Tea polyphenol modified, photothermal responsive and ROS generative black phosphorus quantum dots as nanoplatforms for promoting MRSA infected wounds healing in diabetic rats. *J Nanobiotechnol* 2021; 19: 362.
- Liu X, Gaihre B, George MN, et al. 2D phosphorene nanosheets, quantum dots, nanoribbons: synthesis and biomedical applications. *Biomater Sci* 2021; 9: 2768–2803.

24. Qian Y, Yuan WE, Cheng Y, et al. Concentrically integrative bioassembly of a three-dimensional black phosphorus nanoscaffold for restoring neurogenesis, angiogenesis, and immune homeostasis. *Nano Lett* 2019; 19: 8990–9001.
25. Frade JM and Ovejero-Benito MC. Neuronal cell cycle: the neuron itself and its circumstances. *Cell Cycle* 2015; 14: 712–720.
26. Lim S and Kaldis P. Cdks, cyclins and CKIs: roles beyond cell cycle regulation. *Development* 2013; 140: 3079–3093.
27. Fry AM, O'Regan L, Sabir SR, et al. Cell cycle regulation by the NEK family of protein kinases. *J Cell Sci* 2012; 125: 4423–4433.
28. Klemm C, Thorpe PH and Ólafsson G. Cell-cycle phosphoregulation of the kinetochore. *Curr Genet* 2021; 67: 177–193.
29. Moura M and Conde C. Phosphatases in mitosis: roles and regulation. *Biomolecules* 2019; 9: 55.
30. Hardwick LJA, Azzarelli R and Philpott A. Cell cycle-dependent phosphorylation and regulation of cellular differentiation. *Biochem Soc Trans* 2018; 46: 1083–1091.
31. Chen W, Ouyang J, Yi X, et al. Black phosphorus nanosheets as a neuroprotective nanomedicine for neurodegenerative disorder therapy. *Adv Mater* 2018; 30: 1703458.
32. Cheriyan T, Ryan DJ, Weinreb JH, et al. Spinal cord injury models: a review. *Spinal Cord* 2014; 52: 588–595.
33. Molina AE, Cristante AF, de Barros TE Sr, et al. A computerized system for the application of Basso, Beattie and Bresnahan scale in Wistar rats. *Acta Ortop Bras* 2015; 23: 179–183.
34. Chang MW, Young MS and Lin MT. An inclined plane system with microcontroller to determine limb motor function of laboratory animals. *J Neurosci Methods* 2008; 168: 186–194.
35. Xie DM, Li YL, Li J, et al. CD51 distinguishes a subpopulation of bone marrow mesenchymal stem cells with distinct migratory potential: a novel cell-based strategy to treat acute myocardial infarction in mice. *Stem Cell Res Ther* 2019; 10: 331.
36. Niu X, Li Y, Shu H, et al. Anomalous size dependence of optical properties in black phosphorus quantum dots. *J Phys Chem Lett* 2016; 7: 370–375.
37. Mu X, Wang JY, Bai X, et al. Black phosphorus quantum dot induced oxidative stress and toxicity in living cells and mice. *ACS Appl Mater Interfaces* 2017; 9: 20399–20409.
38. Gowrishankar S, Yuan P, Wu Y, et al. Massive accumulation of luminal protease-deficient axonal lysosomes at Alzheimer's disease amyloid plaques. *Proc Natl Acad Sci U S A* 2015; 112: E3699–E3708.
39. Han Q, Xie Y, Ordaz JD, et al. Restoring Cellular Energetics promotes axonal regeneration and functional recovery after spinal cord injury. *Cell Metab* 2020; 31: 623–641.e8.
40. McDonald JW and Sadowsky C. Spinal-cord injury. *Lancet* 2002; 359: 417–425.
41. Hutson TH and Di Giovanni S. The translational landscape in spinal cord injury: focus on neuroplasticity and regeneration. *Nat Rev Neurol* 2019; 15: 732–745.
42. Sun MG, Williams J, Munoz-Pinedo C, et al. Correlated three-dimensional light and electron microscopy reveals transformation of mitochondria during apoptosis. *Nat Cell Biol* 2007; 9: 1057–1065.
43. Rintoul GL, Filiano AJ, Brocard JB, et al. Glutamate decreases mitochondrial size and movement in primary forebrain neurons. *J Neurosci* 2003; 23: 7881–7888.
44. Hellenbrand DJ, Quinn CM, Piper ZJ, et al. Inflammation after spinal cord injury: a review of the critical timeline of signaling cues and cellular infiltration. *J Neuroinflammation* 2021; 18: 284.
45. Linnerbauer M, Wheeler MA and Quintana FJ. Astrocyte crosstalk in CNS inflammation. *Neuron* 2020; 108: 608–622.
46. Hart CG and Karimi-Abdolrezaee S. Recent insights on astrocyte mechanisms in CNS homeostasis, pathology, and repair. *J Neurosci Res* 2021; 99: 2427–2462.
47. Schreiner AE, Berlinger E, Langer J, et al. Lesion-induced alterations in astrocyte glutamate transporter expression and function in the hippocampus. *ISRN Neurol* 2013; 2013: 893605.
48. Hara M, Kobayakawa K, Ohkawa Y, et al. Interaction of reactive astrocytes with type I collagen induces astrocytic scar formation through the integrin-N-cadherin pathway after spinal cord injury. *Nat Med* 2017; 23: 818–828.
49. Okada S, Hara M, Kobayakawa K, et al. Astrocyte reactivity and astrogliosis after spinal cord injury. *Neurosci Res* 2018; 126: 39–43.
50. Woods I, O'Connor C, Frugoli L, et al. Biomimetic scaffolds for spinal cord applications exhibit stiffness-dependent immunomodulatory and neurotrophic characteristics. *Adv Healthc Mater* 2022; 11: e2101663.
51. Cua RC, Lau LW, Keough MB, et al. Overcoming neurite-inhibitory chondroitin sulfate proteoglycans in the astrocyte matrix. *Glia* 2013; 61: 972–984.
52. Tran AP, Warren PM and Silver J. The biology of regeneration failure and success after spinal cord injury. *Physiol Rev* 2018; 98: 881–917.
53. Lau LW, Keough MB, Haylock-Jacobs S, et al. Chondroitin sulfate proteoglycans in demyelinated lesions impair remyelination. *Ann Neurol* 2012; 72: 419–432.
54. Choi JK, Park SY, Kim KH, et al. GM-CSF reduces expression of chondroitin sulfate proteoglycan (CSPG) core proteins in TGF- β -treated primary astrocytes. *BMB Rep* 2014; 47: 679–684.
55. Köppe G, Brückner G, Härtig W, et al. Characterization of proteoglycan-containing perineuronal nets by enzymatic treatments of rat brain sections. *Histochem J* 1997; 29: 11–20.
56. Buss A, Pech K, Merkler D, et al. Sequential loss of myelin proteins during Wallerian degeneration in the human spinal cord. *Brain* 2005; 128: 356–364.
57. Baumann N and Pham-Dinh D. Biology of oligodendrocyte and myelin in the mammalian central nervous system. *Physiol Rev* 2001; 81: 871–927.
58. Li N, Yao M, Liu J, et al. Vitamin D promotes remyelination by suppressing c-Myc and inducing oligodendrocyte precursor cell differentiation after traumatic spinal cord injury. *Int J Biol Sci* 2022; 18: 5391–5404.
59. Pukos N, Goodus MT, Sahinkaya FR, et al. Myelin status and oligodendrocyte lineage cells over time after spinal cord injury: What do we know and what still needs to be unwrapped? *Glia* 2019; 67: 2178–2202.

60. Gensel JC, Wang Y, Guan Z, et al. Toll-like receptors and dectin-1, a C-type lectin receptor, trigger divergent functions in CNS macrophages. *J Neurosci* 2015; 35: 9966–9976.
61. Ma J, Li J, Wang X, et al. GDNF-Loaded polydopamine nanoparticles-based anisotropic scaffolds promote spinal cord repair by modulating inhibitory microenvironment. *Adv Healthc Mater* 2023; 12: e2202377.
62. Shen H, Xu B, Yang C, et al. A DAMP-scavenging, IL-10-releasing hydrogel promotes neural regeneration and motor function recovery after spinal cord injury. *Biomaterials* 2022; 280: 121279.
63. Lin S, Xu C, Lin J, et al. Regulation of inflammatory cytokines for spinal cord injury recovery. *Histol Histopathol* 2021; 36: 137–142.
64. Wu J, Stoica BA and Faden AI. Cell cycle activation and spinal cord injury. *Neurother* 2011; 8: 221–228.
65. Gong X, Guan L, Li Q, et al. Black phosphorus quantum dots in inorganic perovskite thin films for efficient photovoltaic application. *Sci Adv* 2020; 6: eaay5661.
66. Zhang W and Liu HT. MAPK signal pathways in the regulation of cell proliferation in mammalian cells. *Cell Res* 2002; 12: 9–18.
67. Franco R, Martínez-Pinilla E, Navarro G, et al. Potential of GPCRs to modulate MAPK and mTOR pathways in Alzheimer's disease. *Prog Neurobiol* 2017; 149–150: 21–38.
68. Hu X, Li R, Wu Y, et al. Thermosensitive heparin-polyoxamer hydrogel encapsulated bFGF and NGF to treat spinal cord injury. *J Cell Mol Med* 2020; 24: 8166–8178.